
ScooBDoob: Schrödinger Bridge with Doob’s h -Transform for Molecular Dynamics

Anonymous Author(s)

Affiliation

Address

email

Abstract

1 The slow processes of stochastic dynamical systems can be captured by Molecular
2 Dynamics (MD) simulations, which approximate transition matrices describing
3 how probabilities evolve over metastable conformations. Standard approaches such
4 as Markov State Models (MSMs) extract dominant conformations and transition
5 statistics via eigendecomposition, but face scalability and generalization limits.
6 Here, we introduce **Schrödinger Bridge with Doob’s h -Transform (ScooBDoob)**,
7 a discrete bridge-matching framework that models metastable dynamics by
8 tilting MSM transition rates through Doob’s transform to generate optimal
9 stochastic paths between prescribed initial and terminal ensembles. We show that
10 ScooBDoob preserves spectral stability of slow modes during training, recovers
11 rare transition pathways with density-aware regularization, and generalizes
12 zero-shot across temperatures. Experiments on the Müller-Brown potential and
13 the Aib9 peptide demonstrate accurate kinetics and robust endpoint-conditioned
14 rollouts, highlighting broad applicability to biomolecular dynamics.

15 1 Introduction

16 Simulating molecular dynamics (MD) trajectories accurately and efficiently remains a fundamental
17 challenge in computational chemistry, particularly when predicting rare transition events between
18 metastable states [Lewis et al., 2025a]. Such events are crucial for understanding biological processes
19 like protein folding, ligand binding, and conformational dynamics, but occur over long timescales,
20 making direct computational simulations prohibitively expensive [Ghosh and Ranjan, 2020, Vincoff
21 et al., 2025]. Markov State Models (MSMs) have emerged as a popular approach for approximating
22 these slow processes by representing continuous trajectories as discrete microstates and modeling
23 transitions between these states as Markovian jumps [Chodera and Noé, 2014, Trubiano and Hagan,
24 2024, Pande et al., 2010]. By deriving transition probability matrices from MD data, MSMs efficiently
25 summarize long-term dynamical behavior, significantly reducing computational complexity and
26 enabling more tractable analysis of complex biomolecular systems [Chodera and Noé, 2014, Trubiano
27 and Hagan, 2024, Pande et al., 2010].

28 However, MSMs face substantial challenges in practice. First, eigendecomposition of transition
29 matrices is a crucial step for extracting dynamical information, but can lead to numerical instability
30 and inaccuracies if eigenvectors are unconstrained [Frank et al., 2022]. Unstable eigenvectors can
31 produce physically unrealistic predictions, which undermines the reliability of MSMs for critical
32 biological applications. Furthermore, MD simulation data is inherently sparse in regions of confor-
33 mational space that correspond to rare transitions, resulting in poorly estimated transition probabilities
34 and limited predictive accuracy [Konovalov et al., 2021, Frank et al., 2022]. Sparse data render
35 MSM-derived trajectories highly sensitive to sampling variability and noise, thereby limiting their
36 generalizability to unseen conformations and conditions.

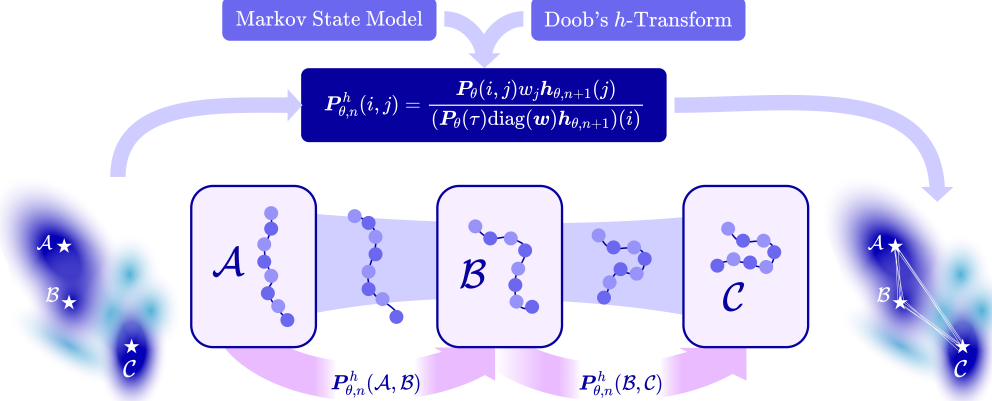


Figure 1: **Schrödinger Bridge with Doob’s h -Transform (ScooBDoob).** ScooBDoob models stochastic transition paths between metastable states by learning Markov State Models (MSMs) of molecular dynamics trajectories and conditioning on target end-states using Doob’s h -Transform.

37 Recent methods have leveraged generative models to sample transition paths between metastable
 38 states by framing trajectory generation as a stochastic control problem. These approaches include
 39 optimization of the Onsager-Machlup (OM) functional or a related control Lagrangian to produce
 40 high-likelihood paths under learned dynamics [Raja et al., 2025, Du et al., 2024], and diffusion-based
 41 samplers trained with off-policy learning to efficiently approximate the transition path distribution
 42 [Seong et al., 2025, Holdijk et al., 2023]. More broadly, Schrödinger bridge formulations [Liu
 43 et al., 2023] provide a principled framework for path sampling under endpoint constraints, and recent
 44 advances in stochastic optimal control further connect bridge problems to tractable learning objectives
 45 [Liu et al., 2025]. Collectively, these methods demonstrate the promise of conditioning generative
 46 dynamics on endpoint constraints to study rare events, bypassing the need for collective variables or
 47 retraining on system-specific data.

48 In this work, we introduce **Schrödinger Bridge with Doob’s h -Transform (ScooBDoob)**, a novel
 49 Schrödinger bridge formulation explicitly designed to enhance the robustness, stability, and general-
 50 ization capabilities of MSM-based methods. Our framework integrates three key advancements:

- 51 1. **Parameterization of the Doob-Tilted Transition Matrix.** To condition the transition path
 52 on a target meta-stable state, we leverage Doob’s h -transform to tilt the unconditional MSM
 53 transition matrix and train our parameterized model to match the optimal Schrödinger bridge.
 54 This enables the efficient simulation of feasible transition paths despite energy barriers.
- 55 2. **Density-Aware Regularization.** We introduce density-aware reweighting, which adjusts
 56 transition probabilities based on empirical MD sampling density, significantly enhancing
 57 robustness against data sparsity and sampling variability.
- 58 3. **Stiefel-Constrained Eigenvector Optimization.** We explicitly constrain eigenvectors to the
 59 Stiefel manifold, ensuring numerical stability and physically meaningful directional transitions,
 60 thus addressing the instability associated with unconstrained eigendecompositions.

61 We provide a detailed discussion on related works in Appendix A.

62 2 ScooBDoob: Schrödinger Bridge with Doob’s h -Transform

63 We introduce **Schrödinger Bridge with Doob’s h -Transform (ScooBDoob)**, a discrete Schrödinger
 64 bridge framework that learns stochastic transitions between metastable states in molecular systems
 65 using a Doob-transformed Markov State Model (MSM). ScooBDoob is capable of modelling discrete
 66 transition probabilities between MD microstates without requiring knowledge of the underlying
 67 potential energy landscape, enabling flexible generalization to molecular systems without known
 68 energies and sparse MD data.

Algorithm 1 ScooBDoob: Schrödinger Bridge with Doob's h -Transform

```

1: Input: Observed count of transitions  $i \rightarrow j$  at  $\tau$  lag  $C(i, j; \tau)$  for all  $i, j \in \{1, \dots, m\}$ 
2: while Training do
3:    $\mathbf{P}_{ij}(\tau) \leftarrow \frac{C(i, j; \tau)}{\sum_{j'} C(i, j'; \tau)}$ ,  $\mathbf{P}(\tau) \leftarrow [\mathbf{P}_{ij}(\tau)]$ 
4:    $\mathbf{V}(i) \leftarrow \alpha/(C_i + 1)$ ,  $\mathbf{w}(i) \leftarrow \exp(-\tau \mathbf{V}(i))$  ▷ density-aware weights
5:    $\mathbf{h}_N^V \leftarrow \nu$  ▷ initialize terminal condition
6:   for  $n$  in  $N - 1, \dots, 0$  do
7:      $\mathbf{h}_n^V \leftarrow \mathbf{P}(\tau)(\text{diag}(\mathbf{w})\mathbf{h}_{n+1}^V)$  ▷ compute tilted distributions
8:      $\mathbf{P}_n^V(i, j) \leftarrow \frac{\mathbf{P}_{ij}(\tau)\mathbf{w}(j)\mathbf{h}_{n+1}^V(j)}{(\mathbf{P}(\tau)\text{diag}(\mathbf{w})\mathbf{h}_{n+1}^V(i))}$ ,  $\mathbf{P}_n^V \leftarrow [\mathbf{P}_n^V(i, j)]$ 
9:
10:  end for
11:  for micro-state  $i$  in  $1, \dots, m$  do ▷ train generator for each state  $i$ 
12:     $\mathbf{P}_{n,\theta}^h(i, \cdot) \leftarrow \text{NN}(\theta)$ 
13:    Compute loss  $\mathcal{L}_{\text{total}}(\theta) = \mathcal{L}_{\text{MSM}}(\theta) + \gamma_{\text{bridge}}\mathcal{L}_{\text{bridge}}(\theta) + \gamma_{\text{stief}}\mathcal{L}_{\text{stief}}(\theta)$ 
14:    Optimize  $\theta$  with  $\nabla_{\theta}\mathcal{L}_{\text{total}}$ 
15:  end for
16: end while
17: return parameterized transition predictor  $\mathbf{P}_{\theta}(\tau) : [0, 1] \rightarrow \mathbb{R}^{m \times m}$ 

```

69 **2.1 Problem Setup**

70 While MD is critical for exploring conformational landscapes and reaction pathways of biomolecular
71 systems, the performance is hindered by two prominent challenges. First, MD requires **well-defined**
72 and **transferable force fields** that accurately capture intermolecular and intramolecular forces
73 [Kaminski and Jorgensen, 1996, Zhu et al., 2012]. While classical force fields enable fast simulations,
74 they rely on several assumptions that limit the expressivity of the simulation to model rare or
75 heterogeneous phenomena. ML-based force fields increase expressivity [Arts et al., 2023, Charron
76 et al., 2025, Lewis et al., 2025b]; however, they are biased towards the interactions seen in the training
77 data and remain limited in their ability to generalize to unseen systems.

78 Second, many crucial processes, such as protein folding and allosteric switches, occur between
79 multiple low-energy, *meta-stable states*, where transitions away from the state are rare and occur
80 over long time-scales [Noé and Clementi, 2017]. This makes these **rare processes prohibitively**
81 **expensive to simulate**, especially for larger systems. Techniques that aim to coerce these transitions
82 over smaller timescales [Ensing et al., 2006, Branduardi et al., 2012, Bussi and Branduardi, 2015,
83 Ghosh and Ranjan, 2020] often undermine the probabilistic nature of these transitions and miss
84 intermediate states.

85 These challenges motivate the development of **data-centric approaches for learning MD trajec-**
86 **tories** [Jing et al., 2024, Daigavane et al., 2025, Lu et al., 2025, Tan et al., 2025, Rehman et al., 2025,
87 Wang et al., 2024] that bypass the need for defined energy landscapes and can generate feasible
88 maps between meta-stable states that align with the data manifold, while accounting for the sparsity
89 of MD data. Notably, **ScooBDoob** addresses *all* of these challenges by (1) learning probabilistic
90 transition rates *directly* from MD trajectory data, bypassing the need for external force-fields, (2)
91 conditioning discrete transitions on target states grounded in Doob's h -Transform theory, and (3)
92 amplifying regions of low data density with Feynman-Kac reweighting.

93 **2.2 Defining Endpoint-Conditioned Transitions Between Meta-Stable States**

94 **Doob's h -Transform for Target-Conditioned Transition Rates** Given an unconditional transition
95 matrix $\mathbf{P}(\tau) \in \mathbb{R}^{m \times m}$, we can steer trajectories toward a terminal distribution $\nu \in \Delta^{m-1}$ over
96 $T = N\tau$ steps by recursively define the distribution at each step $\mathbf{h}_n \in \Delta^{m-1}$ backward in time.

$$\mathbf{h}_N = \nu, \quad \mathbf{h}_n = \mathbf{P}(\tau)\mathbf{h}_{n+1}, \quad n \in \{N-1, \dots, 0\}. \quad (1)$$

97 Then, we construct the time-dependent Doob-conditioned transition matrix as

$$\mathbf{P}_n^h(i, j) = \mathbf{P}_{ij}(\tau) \frac{\mathbf{h}_{n+1}(j)}{\mathbf{h}_n(i)}, \quad \sum_{j=1}^m \mathbf{P}_n^h(i, j) = 1. \quad (2)$$

98 **Density-Aware Regularization via Feynman-Kac for Sparse MD Data** To mitigate bias toward
 99 over-sampled basins and encourage coverage of sparsely visited regions, we introduce a density-aware
 100 non-negative potential for each micro-state $\mathbf{V} : \{1, \dots, m\} \rightarrow \mathbb{R}_{\geq 0}$ proportional to the empirical
 101 outgoing transition density.

$$C_i = \sum_{j \neq i} C_{ij}(\tau), \quad \rho(i) = \frac{\max(C_i, 1)}{\bar{C}}, \quad \mathbf{V}(i) = \alpha \rho(i), \quad (3)$$

102 where $C_{ij}(\tau)$ is the number of observed MD transitions at lag τ from state i to state j and C_i denotes
 103 the total number of outgoing transitions from state i . \bar{C} is the mean of C_i . $\alpha \geq 0$ is a hyperparameter
 104 controlling the penalization of sparsely sampled transitions. With the potential, we define a weight
 105 vector $\mathbf{w} \in \mathbb{R}^m$ containing the weights of each microstate $w_j = \exp(-\tau \mathbf{V}(j))$.

106 Given a time horizon of $T = N\tau$ with target distribution $\nu \in \Delta^{m-1}$, we define the target-conditioned
 107 density-aware probability distributions $\mathbf{h}_n^V \in \Delta^{m-1}$ at each time increment from $n \in \{N, N-1, \dots, 0\}$ as
 108

$$\mathbf{h}_N^V = \nu, \quad \mathbf{h}_n^V = \mathbf{P}(\tau) \left(\text{diag}(\mathbf{w}) \mathbf{h}_{n+1}^V \right) \quad (4)$$

109 where $\text{diag}(\mathbf{w}) \mathbf{h}_{n+1}^V$ reweights the probability of each state at time $n+1$ by its corresponding density
 110 weight w_j , thereby encouraging the likelihood of transitioning into sparsely sampled intermediate
 111 states. The resulting density-aware Doob kernel at each time step $n \in \{1, \dots, N\}$ is defined as

$$\mathbf{P}_n^h(i, j) = \frac{\mathbf{P}_{ij}(\tau) w_j \mathbf{h}_{n+1}^V(j)}{(\mathbf{P}(\tau) \text{diag}(\mathbf{w}) \mathbf{h}_{n+1}^V)(i)}, \quad \sum_{j=1}^m \mathbf{P}_n^h(i, j) = 1 \quad (5)$$

112 Increasing the value of α used to compute \mathbf{V} strengthens the regularization, further discouraging
 113 paths through low-density states. Setting $\alpha = 0$ recovers the standard Doob kernel without density
 114 adjustment.

Proposition 2.1 (ScooBDoob yields the target end state for one-hot ν). *Assume the terminal distribution is the one-hot vector $\nu = \mathbf{e}_z$ concentrating all mass on a fixed target microstate z . Let \mathbf{h}_n (or \mathbf{h}_n^V) be defined by the backward recursions above and let \mathbf{P}_n^h be the corresponding Doob kernels. For any initial distribution μ_0 supported on $\{i : \mathbf{h}_0(i) > 0\}$, the forward evolution*

$$\mu_{n+1} = \mu_n \mathbf{P}_n^h, \quad n = 0, 1, \dots, N-1$$

115 at terminal time satisfies $\mu_N = \nu$.

116 **Stiefel Manifold Constraint for Large Systems** To enable stable eigendecomposition of the
 117 transition matrix and enforce orthonormality of the learned eigenvectors, we begin by constructing
 118 the symmetrized form of the Markov State Model. Let $\mathbf{P}(\tau) \in \mathbb{R}^{m \times m}$ have stationary distribution $\boldsymbol{\pi}$
 119 with $\mathbf{D} = \text{diag}(\boldsymbol{\pi})$, and define the reversible symmetrization

$$\mathbf{M} = \mathbf{D}^{1/2} \mathbf{P}(\tau) \mathbf{D}^{-1/2} = \mathbf{Q}_{\text{MSM}} \boldsymbol{\Lambda}_{\text{MSM}} \mathbf{Q}_{\text{MSM}}^\top, \quad (6)$$

120 where $\mathbf{Q}_{\text{MSM}} \in \mathbb{R}^{m \times r}$ has orthonormal columns and $\boldsymbol{\Lambda}_{\text{MSM}} = \text{diag}(\lambda_1, \dots, \lambda_r)$ collects the top r
 121 modes ($r = m$ gives the full basis). We maintain orthonormal columns by constraining \mathbf{Q}_{MSM} to
 122 the Stiefel manifold $\mathcal{S}_{m,r}$ defined by

$$\mathbf{Q}_{\text{MSM}} \in \mathcal{S}_{m,r} = \{\mathbf{Q} \in \mathbb{R}^{m \times m} \mid \mathbf{Q}^\top \mathbf{Q} = \mathbf{I}_r\}, \quad (7)$$

123 After a Euclidean update on a chosen objective function \mathcal{L} ,

$$\mathbf{Q}^{(t+1)} = \mathbf{Q}_{\text{MSM}}^{(t)} - \eta \nabla_{\mathbf{Q}_{\text{MSM}}} \mathcal{L}(\mathbf{Q}_{\text{MSM}}^{(t)}), \quad (8)$$

124 with η being a step size. We retract back to $\mathcal{S}_{m,r}$ via a SVD:

$$\mathbf{Q}^{(t+1)} = \mathbf{U} \boldsymbol{\Sigma} \mathbf{V}^\top, \quad \mathbf{U}^\top \mathbf{U} = \mathbf{V}^\top \mathbf{V} = \mathbf{I} \quad (9)$$

125 where $\boldsymbol{\Sigma} = \text{diag}(\sigma_1, \dots, \sigma_k)$. This ensures that the transition matrix \mathbf{Q}_{MSM} remains orthonormal
 126 while steering the kinetics towards the target state.

127 **2.3 Learning Transition Dynamics from Markov State Models**

128 To learn the optimal discrete bridges over microstates, we treat the empirical MSM transition matrix
129 $\mathbf{P}_{\text{ref}}(\tau) \in \mathbb{R}^{m \times m}$ as the fixed reference dynamics. We match the reference dynamics with a one-step
130 parameterized network $\mathbf{P}_\theta(\tau)$ that is row-stochastic, and define a sequence of time-dependent tilted
131 transition matrices with Doob's h -transform. Finally, we learn a time-dependent network that predicts
132 the tilted transition probabilities $\mathbf{P}_{\theta,n}^h$ which preserve the MSM structure via a Stiefel manifold
133 constraint. The full training procedure is provided in Algorithm 2.

134 **Parameterization of the Discrete Transition Matrices** Let $\mathbf{P}_\theta(\tau) \in \mathbb{R}^{m \times m}$ be the learned
135 one-step transition matrix. Let z_θ be a neural network that produces a positive endpoint potential;
136 define

$$\mathbf{h}_{\theta,N} = \nu, \quad \mathbf{h}_{\theta,n} = \mathbf{P}_\theta(\tau) \text{diag}(\mathbf{w}) \mathbf{h}_{\theta,n+1}, \quad n \in \{N-1, \dots, 0\}. \quad (10)$$

137 with density-aware regularization $w_j = \exp(-\tau \mathbf{V}(j))$ introduced in Section 2.2. The student's
138 time-inhomogeneous kernels are the discrete Doob tilts:

$$\mathbf{P}_{\theta,n}^h(i, j) = \frac{\mathbf{P}_\theta(i, j) w_j \mathbf{h}_{\theta,n+1}(j)}{(\mathbf{P}_\theta(\tau) \text{diag}(\mathbf{w}) \mathbf{h}_{\theta,n+1})(i)}, \quad \sum_{j=1}^m \mathbf{P}_{\theta,n}^h(i, j) = 1. \quad (11)$$

139 **2.4 Defining the Training Objective**

140 **Unconditional MSM Loss** Let $C_{ij}(\tau)$ denote the empirical transition counts at lag τ and $\mathbf{P}_\theta(\tau) \in$
141 $\mathbb{R}^{m \times m}$ be a parameterized network. We train \mathbf{P}_θ with an unconditional MSM loss \mathcal{L}_{MSM} defined as

$$\mathcal{L}_{\text{MSM}} = - \sum_{i,j} C_{ij}(\tau) \log \mathbf{P}_{\theta,ij}(\tau) + \gamma_{\text{CK}} \mathcal{L}_{\text{CK}} + \gamma_{\text{rev}} \mathcal{L}_{\text{rev}} \quad (12)$$

$$\mathcal{L}_{\text{CK}} = \sum_{k=2}^K \left\| \widehat{\mathbf{P}}(k\tau) - \mathbf{P}_\theta(\tau)^k \right\|_F^2, \quad \mathcal{L}_{\text{rev}} = \left\| \mathbf{D}_\theta \mathbf{P}_\theta(\tau) - \mathbf{P}_\theta(\tau)^\top \mathbf{D}_\theta \right\|_F^2 \quad (13)$$

142 where $\boldsymbol{\pi}_\theta^\top \mathbf{P}_\theta(\tau) = \boldsymbol{\pi}_\theta^\top$ and $\mathbf{D}_\theta = \text{diag}(\boldsymbol{\pi}_\theta)$, and $K \in \{2, 3\}$ in practice. The first term represents
143 the count likelihood, and the second and third terms are the Chapman-Kolmogorov (CK) consistency
144 and reversibility, respectively.

145 **Schrödinger Bridge Loss** To train $\mathbf{P}_{\theta,n}^h$ such that it predicts the optimal Schrödinger bridge defined
146 by tilting the reference dynamics with Doob's h -transform, we minimize a KL-divergence-based
147 bridge loss $\mathcal{L}_{\text{bridge}}$ defined as

$$\mathcal{L}_{\text{bridge}} = \sum_{n=0}^{N-1} \sum_{i=1}^m \text{KL} \left(\mathbf{P}_{\text{ref},n}^h(i, \cdot) \middle\| \mathbf{P}_{\theta,n}^h(i, \cdot) \right) \quad (14)$$

148 where $\mathbf{P}_{\text{ref},n}^h(i, \cdot)$ is defined with (5) using the fixed reference dynamics $\mathbf{P}_{\text{ref}}(\tau)$

149 **Stiefel Loss** Given the parameterized transition matrix $\mathbf{P}_\theta(\tau)$, we obtain the top- r eigenvector-
150 eigenvalue pairs by symmetrizing and diagonalizing $\mathbf{M}_\theta \approx \mathbf{Q}_\theta \boldsymbol{\Lambda}_\theta \mathbf{Q}_\theta^\top$, $\mathbf{Q}_\theta \in \mathbb{R}^{m \times r}$ (See Appendix
151 B.3 for full details). To ensure that the eigenvectors are orthonormal, we add a soft Stiefel loss $\mathcal{L}_{\text{stief}}$
152 defined as

$$\mathcal{L}_{\text{stief}} = \left\| \mathbf{Q}_\theta^\top \mathbf{Q}_\theta - \mathbf{I}_r \right\|_F^2 + \eta \sum_{i=1}^r \max(0, |\lambda_{\theta,i}| - 1)^2 \quad (15)$$

153 We show in Figure A1 that the orthonormal constraint is enforced throughout training, highlighting
154 that our approach effectively preserves the validity of the learned transition matrix. Finally, we define
155 the **total training loss** to be the weighted sum of the MSM loss, bridge loss, and Stiefel loss, given by

$$\mathcal{L}_{\text{total}} = \mathcal{L}_{\text{MSM}} + \gamma_{\text{bridge}} \mathcal{L}_{\text{bridge}} + \gamma_{\text{stief}} \mathcal{L}_{\text{stief}} \quad (16)$$

156 which jointly optimizes the one-step transition matrix (teacher model) and the time-varying condi-
157 tional transition dynamics.

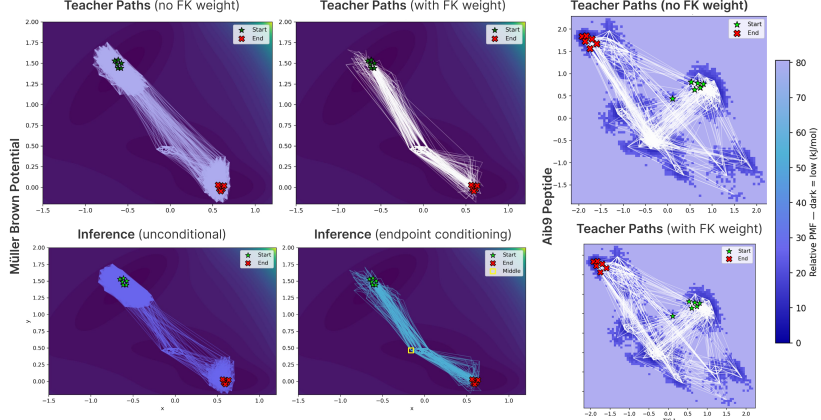


Figure 2: **Transition Paths Predicted by ScooBDoob on Müller-Brown Potential and Aib9 Peptide.** We show the teacher paths with and without density-aware FK reweighting. The inference paths are shown for the MB potential with and without endpoint conditioning.

158 2.5 Simulating the Learned Transition Dynamics

159 **Simulating Unconditional Dynamics** Given an initial distribution over microstates $\mu_0 \in \Delta^{m-1}$,
160 we can simulate the unconditional trajectory over time $T = N\tau$ with the learned reference transition
161 matrix $\mathbf{P}_\theta(\tau)$.

$$\mu_n = \mu_0 \mathbf{P}_\theta(\tau)^n, \quad \mathbf{x}_{n+1} \sim \mathbf{P}_\theta(\tau)(\mathbf{x}_n, \cdot) \quad (17)$$

162 **Target Conditioned Bridge** Given a time horizon $T = N\tau$ and a target distribution $\nu \in \mathbb{R}^m$, we
163 can sample the intermediate trajectory from an initial distribution $\mu_0 \in \Delta^{m-1}$

$$\mu_{n+1} = \mu_n \mathbf{P}_{\theta,n}^h \quad \text{or} \quad \mathbf{x}_{n+1} \sim \mathbf{P}_{\theta,n}^{(h,V)}(\mathbf{x}_n, \cdot). \quad (18)$$

164 over time steps $n \in \{1, \dots, N\}$. Unconditional and target-conditioned simulation proceeds via
165 Algorithm 3.

166 3 Experiments

167 Here, we demonstrate the effectiveness of **ScooBDoob** on predicting discrete transitions between MD
168 states conditioned on a target state. We start with a synthetic example on the Müller-Brown (MB)
169 potential energy landscape, illustrating the model’s ability to capture intermediate states between
170 conditioned endpoints. Then, we scale our evaluation to the 9-residue α -helical Aib9 peptide with
171 two distinct intermediate paths [Karle and Bala, 1990].

172 3.1 Müller-Brown Potential

173 **Setup** Following [Müller and Brown, 1979], we build up the testing system for a 2D Müller-Brown
174 potential with a potential energy landscape $U(\mathbf{x})$ with three local minima states. We generated 8
175 unconditioned rollouts of length 8000 steps each, seeding half of the trajectories near the starting
176 point at $(-0.6, 1.5)$, and the other half near the end point at $(0.6, 0.0)$. 64K frames are used for
177 training in total. Experiment details are given in Appendix E.

178 **Results** Using TICA with lag $\tau = 120$ steps, we discretize trajectories into $K = 200$ microstates. The reference MSM exhibits a spectral
179 gap with $\lambda_2 = 0.986$, indicating slow transitions. We first constructed
180 our FK-Doob teacher with density-aware weights and committor-
181 based biasing to enable transition paths to cross saddle points. After
182 training a parameterized student kernel, we found that the unconditional
183 path explored essential states, while conditioning on the target
184 end state significantly reduced the search space and produced more

Table 1: **Results for Müller Brown potential with $N = 60$.**

Metric	MB potential
Row-KL (\downarrow)	0.3204
CK (\downarrow)	0.5401
Mean \mathcal{W}_2 (\downarrow)	0.2038

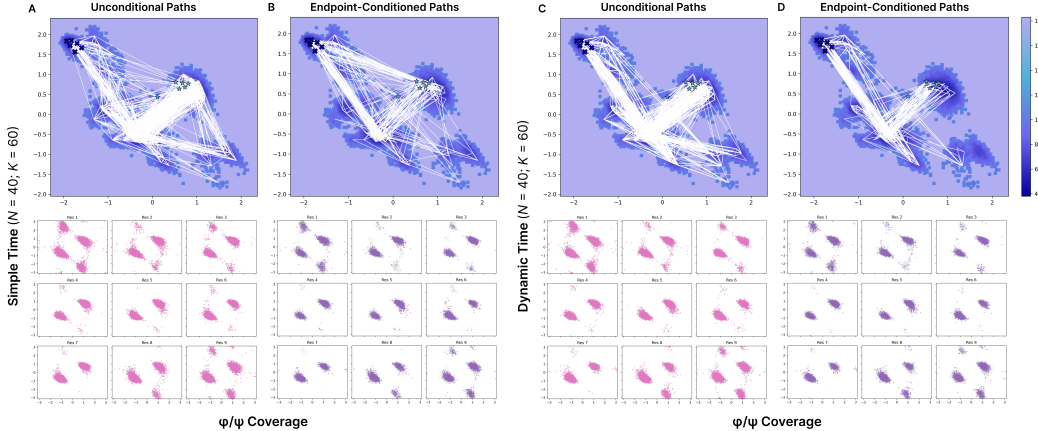


Figure 3: Simulated transition paths for Aib9 Peptide. Simple time indicates a fixed lag time $\tau = 60$, and dynamic time indicates a non-fixed lag time, N indicates the number of jumps simulated at inference, and K denotes the number of discrete microstates. Dark purple indicates high probability mass, and light purple indicates low probability mass. The axes are the φ/ψ dihedral angles. **(A)** Unconditional paths simulated for 60 jumps. **(B)** Endpoint-conditioned paths with Doob's h -transform simulated with $\tau = 60$. **(C)** Unconditional paths and **(D)** endpoint-conditioned paths simulated from dynamic τ .

186 concentrated endpoints (Figure 3, Table 1). To test generalization,
 187 we evaluated zero-shot performance across $N \in \{5, 55, 120\}$. The
 188 student kernel adapted well for $N = 55$ and $N = 120$, but for the extreme case of $N = 5$, it failed
 189 to consistently cross saddle points. This suggests that careful selection of N is critical to ensure
 190 sufficient exploration time (Figure A3).

191 3.2 Aib9 Peptide

192 **Setup** Aib9 peptide is a 9-residue peptide experimentally validated to have two known macro
 193 intermediate states. We retrieve the Aib9 peptide trajectory with 100 ns simulation length from [Wang
 194 and Tiwary, 2021]. We picked the replica at 400K for training and 412K for zero-shot prediction.
 195 There are a total of 50K frames, and 70% are used for training.

196 **Results** We selected the 400K replica as our training trajectory and built ScooBDoob on the
 197 TICA-projected microstates of the Aib9 peptide using τ sweeping based on a balance selection
 198 from the spectral gap against CK error. The teacher kernel, trained with FK constraints, produced
 199 smoother and more connected transition paths (Figure 3). In addition to matching MSM metrics
 200 (Table 2), we mapped transitions back to the original ψ/ϕ angle distributions and verified that the
 201 correct intermediate states participated in the transitions with high probability.

202 The lag time τ and the number of clusters K contribute most strongly to the quality of the sampled
 203 paths. With a larger K , the model has more possible microstate transitions, which increases its ability
 204 to reach rare states. Conversely, a smaller K makes the number of microstates closer to the number
 205 of macrostates, effectively coarsening the dynamics. With the additional of the desired end state
 206 signal during inference, the paths will guarantee to end at the endpoints, as demonstrated in the
 207 Figure 3. When comparing fixed and dynamic timesteps, the dynamic variant produces paths that
 208 visually follow the teacher more closely, often finding multiple reasonable routes to the endpoint. By
 209 contrast, the fixed variant sometimes finds the shortcut to the endpoints and involve some looping
 210 between nearby states, as shown by the higher density of the white paths chosen between some states.
 211 Although the fixed N yields lower row-KL and endpoint KL numerically, these scores often reflect
 212 confident transitions rather than a more faithful path exploration follows the teacher.

213 In addition, we noticed that during inference, when $N = K$, the end point KL divergence spikes,
 214 even though other metrics remain comparable. We suspect that the model effectively compressed the
 215 dynamics so that the probability mass arrives at the endpoints either too quickly or along the wrong
 216 support. This creates an artificial divergence in the endpoint distribution, even though the rollout
 217 paths still appear reasonable.

Table 2: **Ablation studies for Aib9 experiment hyperparameters.** Metrics are computed for inference rollouts. Total steps N determine the step choices for the models. The number of nearest neighbors K determines the number of discrete microstates that can be transitioned into. Simple timestep defines a rigid number of steps, and dynamic timesteps allow various timesteps.

Hyperparameter	Row-KL (\downarrow)	CK (\downarrow)	Mean \mathcal{W}_2 (\downarrow)	KL _{endpoint} (\downarrow)
Total Steps N at fixed $K = 40$				
$N = 20$	0.48 ± 0.08	0.67	0.032	1.09 ± 0.01
$N = 40$	0.40 ± 0.06	0.66	0.19	11.17 ± 0.04
$N = 60$	0.46 ± 0.08	0.67	0.053	0.88 ± 0.02
Nearest Neighbor K at fixed $N = 60$				
$K = 40$	0.45 ± 0.08	0.64	0.05	0.82 ± 0.02
$K = 60$	0.42 ± 0.07	0.67	0.19	10.78 ± 0.04
$K = 100$	0.48 ± 0.08	0.63	0.040	0.86 ± 0.02
Timestep $N = 40, K = 60$				
Simple	0.26 ± 0.07	0.49	0.0008	0.42 ± 0.01
Dynamic	0.46 ± 0.08	0.67	0.053	0.88 ± 0.02

218 To monitor spectral stability during training, we evaluated the leading eigenvalues and eigenvectors
 219 of the learned transition matrix P_θ at each epoch (Table A2, Figure A1). The dominant eigenvalue λ_1
 220 remained near 1, as required for MSMs, and eigenvalue equation residuals were negligible, confirming
 221 numerical accuracy. Successive eigenvectors showed overlaps approaching 1 with small Frobenius
 222 distances, indicating smooth evolution and stable slow modes. These diagnostics confirm that Stiefel
 223 regularization stabilizes the eigendecomposition during training.

224 We also tested zero-shot generalization on replicas at $412K$ and $503K$ (Table A1). The fixed- N
 225 kernel achieved lower row-KL under temperature shift by concentrating transitions into sharper steps,
 226 while the multi- N kernel spread probability more smoothly across paths. This smoothing raised
 227 row-KL slightly but kept CK error low, showing that multi- N training preserves overall kinetics and
 228 yields more robust rollouts at unseen temperatures despite less favorable local scores.

229 4 Conclusion

230 We have introduced **Schrödinger Bridge with Doob’s h -Transform (ScooBDoob)**, a machine learning
 231 framework for modeling molecular dynamics trajectories by learning discrete transitions between
 232 metastable states. ScooBDoob constructs a principled Schrödinger bridge from empirical MSMs
 233 using Doob’s transform and density-aware regularization, enabling rare-event trajectory generation
 234 without a known energy landscape. This approach allows conditioning on endpoint structures, making
 235 it well-suited for applications like protein refolding, allosteric modulation, and conformational control.
 236 Our future extensions will incorporate experimental intermediates or kinetic priors as constraints,
 237 enabling multi-objective control over long-timescale dynamics in undersampled or sparse regimes.

238 **References**

239 Sarah Lewis, Tim Hempel, José Jiménez-Luna, Michael Gastegger, Yu Xie, Andrew YK Foong,
240 Victor García Satorras, Osama Abdin, Bastiaan S Veeling, Iryna Zaporozhets, et al. Scalable
241 emulation of protein equilibrium ensembles with generative deep learning. *Science*, page eadv9817,
242 2025a.

243 Debasish Kumar Ghosh and Akash Ranjan. The metastable states of proteins. *Protein Science*, 29(7):
244 1559–1568, 2020.

245 Sophia Vincoff, Shrey Goel, Ksenia Kholina, Rishab Pulugurta, Pranay Vure, and Pranam Chatterjee.
246 Fuson-plm: a fusion oncoprotein-specific language model via adjusted rate masking. *Nature
247 Communications*, 16(1):1436, 2025.

248 John D Chodera and Frank Noé. Markov state models of biomolecular conformational dynamics.
249 *Current opinion in structural biology*, 25:135–144, 2014.

250 Anthony Trubiano and Michael F Hagan. Markov state model approach to simulate self-assembly.
251 *Physical Review X*, 14(4):041063, 2024.

252 Vijay S Pande, Kyle Beauchamp, and Gregory R Bowman. Everything you wanted to know about
253 markov state models but were afraid to ask. *Methods*, 52(1):99–105, 2010.

254 Anna-Simone Frank, Alexander Sikorski, and Susanna Röblitz. Spectral clustering of markov chain
255 transition matrices with complex eigenvalues. *arXiv preprint arXiv:2206.14537*, 2022.

256 Kirill A Konovalov, Ilona Christy Unarta, Siqin Cao, Eshani C Goonetilleke, and Xuhui Huang.
257 Markov state models to study the functional dynamics of proteins in the wake of machine learning.
258 *JACS Au*, 1(9):1330–1341, 2021.

259 Sanjeev Raja, Martin Sipka, Michael Psenka, Tobias Kreiman, Michal Pavelka, and Aditi S. Krish-
260 napriyan. Action-minimization meets generative modeling: Efficient transition path sampling with
261 the onsager-machlup functional. In *Forty-second International Conference on Machine Learning*,
262 2025.

263 Yuanqi Du, Michael Plainer, Rob Brekelmans, Chenru Duan, Frank Noe, Carla P Gomes, Alan
264 Aspuru-Guzik, and Kirill Neklyudov. Doob’s lagrangian: A sample-efficient variational approach
265 to transition path sampling. In *The Thirty-eighth Annual Conference on Neural Information
266 Processing Systems*, 2024.

267 Kiyoung Seong, Seonghyun Park, Seonghwan Kim, Woo Youn Kim, and Sungsoo Ahn. Transition
268 path sampling with improved off-policy training of diffusion path samplers. In *The Thirteenth
269 International Conference on Learning Representations*, 2025.

270 Lars Holdijk, Yuanqi Du, Ferry Hooft, Priyank Jaini, Berend Ensing, and Max Welling. Stochastic
271 optimal control for collective variable free sampling of molecular transition paths. *Advances in
272 Neural Information Processing Systems*, 36:79540–79556, 2023.

273 Guan-Horng Liu, Yaron Lipman, Maximilian Nickel, Brian Karrer, Evangelos A. Theodorou, and
274 Ricky T. Q. Chen. Generalized schrödinger bridge matching. *International Conference on Learning
275 Representations*, 2023.

276 Guan-Horng Liu, Jaemoo Choi, Yongxin Chen, Benjamin Kurt Miller, and Ricky TQ Chen. Adjoint
277 schrödinger bridge sampler. *arXiv preprint arXiv:2506.22565*, 2025.

278 George Kaminski and William L Jorgensen. Performance of the amber94, mmff94, and opls-aa force
279 fields for modeling organic liquids. *The Journal of Physical Chemistry*, 100(46):18010–18013,
280 1996.

281 Xiao Zhu, Pedro EM Lopes, and Alexander D MacKerell Jr. Recent developments and applications
282 of the charmm force fields. *Wiley Interdisciplinary Reviews: Computational Molecular Science*, 2
283 (1):167–185, 2012.

284 Marloes Arts, Victor Garcia Satorras, Chin-Wei Huang, Daniel Zugner, Marco Federici, Cecilia
285 Clementi, Frank Noé, Robert Pinsler, and Rianne van den Berg. Two for one: Diffusion models and
286 force fields for coarse-grained molecular dynamics. *Journal of Chemical Theory and Computation*,
287 19(18):6151–6159, 2023.

288 Nicholas E Charron, Klara Bonneau, Aldo S Pasos-Trejo, Andrea Guljas, Yaoyi Chen, Félix Musil,
289 Jacopo Venturin, Daria Gusew, Iryna Zaporozhets, Andreas Krämer, et al. Navigating protein
290 landscapes with a machine-learned transferable coarse-grained model. *Nature chemistry*, pages
291 1–9, 2025.

292 Sarah Lewis, Tim Hempel, José Jiménez-Luna, Michael Gastegger, Yu Xie, Andrew YK Foong,
293 Victor García Satorras, Osama Abdin, Bastiaan S Veeling, Iryna Zaporozhets, et al. Scalable
294 emulation of protein equilibrium ensembles with generative deep learning. *Science*, 389(6761):
295 eadv9817, 2025b.

296 Frank Noé and Cecilia Clementi. Collective variables for the study of long-time kinetics from
297 molecular trajectories: theory and methods. *Current opinion in structural biology*, 43:141–147,
298 2017.

299 Bernd Ensing, Marco De Vivo, Zhiwei Liu, Preston Moore, and Michael L Klein. Metadynamics as a
300 tool for exploring free energy landscapes of chemical reactions. *Accounts of chemical research*, 39
301 (2):73–81, 2006.

302 Davide Branduardi, Giovanni Bussi, and Michele Parrinello. Metadynamics with adaptive gaussians.
303 *Journal of chemical theory and computation*, 8(7):2247–2254, 2012.

304 Giovanni Bussi and Davide Branduardi. Free-energy calculations with metadynamics: Theory and
305 practice. *Reviews in Computational Chemistry Volume 28*, pages 1–49, 2015.

306 Bowen Jing, Hannes Stärk, Tommi Jaakkola, and Bonnie Berger. Generative modeling of molecular
307 dynamics trajectories. *Advances in Neural Information Processing Systems*, 37:40534–40564,
308 2024.

309 Ameya Daigavane, Bodhi P Vani, Darcy Davidson, Saeed Saremi, Joshua A Rackers, and Joseph
310 Kleinhenz. Jamun: Bridging smoothed molecular dynamics and score-based learning for confor-
311 mational ensemble generation. In *ICML 2025 Generative AI and Biology (GenBio) Workshop*.

312 Jiarui Lu, Xiaoyin Chen, Stephen Zhewen Lu, Aurélie Lozano, Vijil Chenthamarakshan, Payel Das,
313 and Jian Tang. Aligning protein conformation ensemble generation with physical feedback. *arXiv*
314 *preprint arXiv:2505.24203*, 2025.

315 Charlie B Tan, Majdi Hassan, Leon Klein, Saifuddin Syed, Dominique Beaini, Michael M Bronstein,
316 Alexander Tong, and Kirill Neklyudov. Amortized sampling with transferable normalizing flows.
317 *arXiv preprint arXiv:2508.18175*, 2025.

318 Danyal Rehman, Oscar Davis, Jiarui Lu, Jian Tang, Michael Bronstein, Yoshua Bengio, Alexander
319 Tong, and Avishek Joey Bose. Fort: Forward-only regression training of normalizing flows. *arXiv*
320 *preprint arXiv:2506.01158*, 2025.

321 Haibo Wang, Yuxuan Qiu, Yanze Wang, Rob Brekelmans, and Yuanqi Du. Generalized flow matching
322 for transition dynamics modeling. *arXiv preprint arXiv:2410.15128*, 2024.

323 Isabella L Karle and Padmanabhan Balaram. Structural characteristics of. alpha.-helical peptide
324 molecules containing aib residues. *Biochemistry*, 29(29):6747–6756, 1990.

325 Klaus Müller and Leo D Brown. Location of saddle points and minimum energy paths by a constrained
326 simplex optimization procedure. *Theoretica chimica acta*, 53:75–93, 1979.

327 Yihang Wang and Pratyush Tiwary. Denoising diffusion probabilistic models for replica exchange.
328 *arXiv preprint arXiv:2107.07369*, 2021.

329 Peter G Bolhuis, David Chandler, Christoph Dellago, and Phillip L Geissler. Transition path sampling:
330 Throwing ropes over rough mountain passes, in the dark. *Annual review of physical chemistry*, 53
331 (1):291–318, 2002.

332 Christoph Dellago, Peter G Bolhuis, Félix S Csajka, and David Chandler. Transition path sampling
333 and the calculation of rate constants. *The Journal of chemical physics*, 108(5):1964–1977, 1998.

334 Eric Vanden-Eijnden et al. Transition-path theory and path-finding algorithms for the study of rare
335 events. *Annual review of physical chemistry*, 61:391–420, 2010.

336 Ferry Hooft, Alberto Perez de Alba Ortiz, and Bernd Ensing. Discovering collective variables of
337 molecular transitions via genetic algorithms and neural networks. *Journal of chemical theory and
338 computation*, 17(4):2294–2306, 2021.

339 Jürgen Schlitter, Michael Engels, and Peter Krüger. Targeted molecular dynamics: a new approach
340 for searching pathways of conformational transitions. *Journal of molecular graphics*, 12(2):84–89,
341 1994.

342 Sergei Izrailev, Sergey Stepaniants, Barry Isralewitz, Dorina Kosztin, Hui Lu, Ferenc Molnar,
343 Willy Wriggers, and Klaus Schulten. Steered molecular dynamics. In *Computational Molecular
344 Dynamics: Challenges, Methods, Ideas: Proceedings of the 2nd International Symposium on
345 Algorithms for Macromolecular Modelling, Berlin, May 21–24, 1997*, pages 39–65. Springer, 1999.

346 Glenn M Torrie and John P Valleau. Nonphysical sampling distributions in monte carlo free-energy
347 estimation: Umbrella sampling. *Journal of computational physics*, 23(2):187–199, 1977.

348 Johannes Kästner. Umbrella sampling. *Wiley Interdisciplinary Reviews: Computational Molecular
349 Science*, 1(6):932–942, 2011.

350 Alessandro Laio and Michele Parrinello. Escaping free-energy minima. *Proceedings of the national
351 academy of sciences*, 99(20):12562–12566, 2002.

352 Jeffrey Comer, James C Gumbart, Jérôme Hénin, Tony Lelièvre, Andrew Pohorille, and Christophe
353 Chipot. The adaptive biasing force method: Everything you always wanted to know but were
354 afraid to ask. *The Journal of Physical Chemistry B*, 119(3):1129–1151, 2015.

355 Michele Invernizzi and Michele Parrinello. Rethinking metadynamics: from bias potentials to
356 probability distributions. *The journal of physical chemistry letters*, 11(7):2731–2736, 2020.

357 Guillermo Pérez-Hernández, Fabian Paul, Toni Giorgino, Gianni De Fabritiis, and Frank Noé.
358 Identification of slow molecular order parameters for markov model construction. *The Journal of
359 chemical physics*, 139(1), 2013.

360 Ronald R Coifman, Stephane Lafon, Ann B Lee, Mauro Maggioni, Boaz Nadler, Frederick Warner,
361 and Steven W Zucker. Geometric diffusions as a tool for harmonic analysis and structure definition
362 of data: Diffusion maps. *Proceedings of the national academy of sciences*, 102(21):7426–7431,
363 2005.

364 Jan-Hendrik Prinz, Hao Wu, Marco Sarich, Bettina Keller, Martin Senne, Martin Held, John D
365 Chodera, Christof Schütte, and Frank Noé. Markov models of molecular kinetics: Generation and
366 validation. *The Journal of chemical physics*, 134(17), 2011.

367 Gregory R Bowman, Vijay S Pande, and Frank Noé. Introduction and overview of this book. In *An
368 introduction to Markov state models and their application to long timescale molecular simulation*,
369 pages 1–6. Springer, 2014.

370 Andreas Mardt, Luca Pasquali, Hao Wu, and Frank Noé. Vampnets for deep learning of molecular
371 kinetics. *Nature communications*, 9(1):5, 2018.

372 Jonas Kohler, Yaoyi Chen, Andreas Kramer, Cecilia Clementi, and Frank Noé. Flow-matching:
373 Efficient coarse-graining of molecular dynamics without forces. *Journal of Chemical Theory and
374 Computation*, 19(3):942–952, 2023.

375 Maciej Majewski, Adrià Pérez, Philipp Thölke, Stefan Doerr, Nicholas E Charron, Toni Giorgino,
376 Brooke E Husic, Cecilia Clementi, Frank Noé, and Gianni De Fabritiis. Machine learning coarse-
377 grained potentials of protein thermodynamics. *Nature Communications*, 14(1):5739, 2023.

378 Alessandro Beghi. On the relative entropy of discrete-time markov processes with given end-point
379 densities. *IEEE Transactions on Information Theory*, 42(5):1529–1535, 2002.

380 Michele Pavon, Francesco Ticozzi, et al. Schrödinger bridges for discrete-time, classical and quantum
381 markovian evolutions. In *Proceedings of the 19th International Symposium on Mathematical*
382 *Theory of Networks and Systems–MTNS*, volume 5, 2010.

383 Michele Pavon and Francesco Ticozzi. Discrete-time classical and quantum markovian evolutions:
384 Maximum entropy problems on path space. *Journal of Mathematical Physics*, 51(4), 2010.

385 Espen Bernton, Jeremy Heng, Arnaud Doucet, and Pierre E Jacob. Schrödinger bridge samplers.
386 *arXiv preprint arXiv:1912.13170*, 2019.

387 Valentin De Bortoli, James Thornton, Jeremy Heng, and Arnaud Doucet. Diffusion schrödinger
388 bridge with applications to score-based generative modeling. *Advances in neural information*
389 *processing systems*, 34:17695–17709, 2021.

390 Jun Hyeong Kim, Seonghwan Kim, Seokhyun Moon, Hyeongwoo Kim, Jeheon Woo, and Woo Youn
391 Kim. Discrete diffusion schrödinger bridge matching for graph transformation. *arXiv preprint*
392 *arXiv:2410.01500*, 2024.

393 Martin K Scherer, Benjamin Trendelkamp-Schroer, Fabian Paul, Guillermo Pérez-Hernández, Moritz
394 Hoffmann, Nuria Plattner, Christoph Wehmeyer, Jan-Hendrik Prinz, and Frank Noé. Pyemma 2: A
395 software package for estimation, validation, and analysis of markov models. *Journal of chemical*
396 *theory and computation*, 11(11):5525–5542, 2015.

397 Helgi I Ingólfsson, Cesar A Lopez, Jaakko J Uusitalo, Djurre H de Jong, Srinivasa M Gopal, Xavier
398 Periole, and Siewert J Marrink. The power of coarse graining in biomolecular simulations. *Wiley*
399 *Interdisciplinary Reviews: Computational Molecular Science*, 4(3):225–248, 2014.

400 Soumil Y Joshi and Sanket A Deshmukh. A review of advancements in coarse-grained molecular
401 dynamics simulations. *Molecular Simulation*, 47(10-11):786–803, 2021.

402 Kyle A Beauchamp, Daniel L Ensign, Rhiju Das, and Vijay S Pande. Quantitative comparison of villin
403 headpiece subdomain simulations and triplet–triplet energy transfer experiments. *Proceedings of*
404 *the National Academy of Sciences*, 108(31):12734–12739, 2011.

405 MRF Smyth. A spectral theoretic proof of perron-frobenius. In *Mathematical Proceedings of the*
406 *Royal Irish Academy*, volume 102, pages 29–35. Royal Irish Academy, 2002.

407 Brooke E Husic and Vijay S Pande. Markov state models: From an art to a science. *Journal of the*
408 *American Chemical Society*, 140(7):2386–2396, 2018.

409 Valeria Simoncini. Variable accuracy of matrix-vector products in projection methods for eigencom-
410 putation. *SIAM journal on numerical analysis*, 43(3):1155–1174, 2005.

411 Susanna Röblitz and Marcus Weber. Fuzzy spectral clustering by pcca+: application to markov state
412 models and data classification. *Advances in Data Analysis and Classification*, 7(2):147–179, 2013.

413 Carlos X Hernández, Hannah K Wayment-Steele, Mohammad M Sultan, Brooke E Husic, and Vijay S
414 Pande. Variational encoding of complex dynamics. *Physical Review E*, 97(6):062412, 2018.

415 **Outline of Appendix**

416 In Appendix B, we discuss the construction of the Markov State Model and the Stiefel manifold
 417 constraint (B.3). Appendix E provides the setup for our experiments and the evaluation metrics.
 418 Finally, the pseudocode for training ScooBDoob is given in Appendix F.

419 **Notation** In this work, we consider a molecular system with features $x(t) \in \mathbb{R}^d$ which can be
 420 reduced with TICA to a lower-dimensional feature vector $y(t)$. We denote the number of microstates
 421 as m and the unconditional transition matrix with lag time τ as $P(\tau) \in \mathbb{R}^{m \times m}$, where $P_{ij}(\tau) \in \mathbb{R}$
 422 is the probability of transition from microstate i at time t to microstate j at time $t + \tau$. This matrix
 423 is constructed from the observed transition counts $C(i, j; \tau) \in \mathbb{R}$. The initial discrete distribution
 424 over the microstates is denoted $\mu_0 \in \Delta^{m-1}$ and the final distribution $\nu \in \Delta^{m-1}$. Given the number
 425 of lag steps N with a total time horizon $T = N\tau$, we define the discrete distribution for step
 426 $n \in \{N-1, \dots, 0\}$ starting from $h_N = \nu \in \Delta^{m-1}$ as $h_n = P(\tau)h_{n+1}$. The Doob-tilted transition
 427 matrices given the backward distributions h_n at each time step n is denoted $P_n^h \in \mathbb{R}^{m \times m}$ where the
 428 transition probability from i to j is $P_n^h(i, j) \in \mathbb{R}$. $V : \{1, \dots, m\} \rightarrow \mathbb{R}_{\geq 0}$ denotes a density-aware
 429 potential for each micro-state which is used to compute a weight vector $w \in \mathbb{R}^m$ where each element
 430 is $w(j) = \exp(-\tau V(j))$.

431 The parameterized unconditional transition matrix with parameters θ is denoted $P_\theta(\tau) \in \mathbb{R}^{m \times m}$
 432 and the corresponding tilted distribution at step n is denoted $h_{\theta, n} \in \mathbb{R}^m$ which constructs the tilted
 433 transition matrix $P_{\theta, n}^h \in \mathbb{R}^{m \times m}$. To define the Stiefel constraint, we symmetrize $P_\theta(\tau)$ with the
 434 diagonal matrix $D = \text{diag}(\pi)$ where $\pi \in \Delta^{m-1}$ is the stationary distribution $\pi^\top P_\theta(\tau) = \pi$ to get
 435 the symmetrical matrix $M \in \mathbb{R}^{m \times m}$. Then, we perform a symmetric eigendecomposition to obtain
 436 the orthonormal matrix $Q_{\text{MSM}} \in \mathbb{R}^{m \times r}$ and eigenvalues $\Lambda_{\text{MSM}} = \text{diag}(\lambda_1, \dots, \lambda_r)$. At inference
 437 time, we generate intermediate distributions $\mu_n \in \Delta^{m-1}$ by applying the learned transition to the
 438 initial distribution μ_0 and sampling discrete states $x_n \sim \mu_n$.

439 **A Related Works**

440 **Transition Path Sampling (TPS)** Computational approaches to transition path sampling over en-
 441 ergy landscapes have been widely explored [Bolhuis et al., 2002, Dellago et al., 1998, Vanden-Eijnden
 442 et al., 2010]. Traditionally, non-ML approaches have leveraged low-dimensional representations
 443 of molecules via *collective variables* (CVs) [Hooft et al., 2021], including steered MD [Schlitter
 444 et al., 1994, Izrailev et al., 1999], umbrella sampling [Torrie and Valleau, 1977, Kästner, 2011],
 445 meta-dynamics [Laio and Parrinello, 2002, Ensing et al., 2006, Branduardi et al., 2012, Bussi and
 446 Branduardi, 2015], adaptive biasing force [Comer et al. 2015], and on-the-fly probability-enhanced
 447 sampling [Invernizzi and Parrinello, 2020]. Such methods are powerful when good CVs are known,
 448 but selecting CVs remains challenging [Hooft et al., 2021].

449 **State-based Kinetic Models** An alternative line of work focuses on *state-based* models that extract
 450 slow kinetics directly from simulation data. A rigorous theory shows that optimal CVs correspond
 451 to the eigenfunctions of the transfer operator underlying MD [Noé and Clementi, 2017]. Practical
 452 approximations include Time-lagged Independent Component Analysis (TICA) [Pérez-Hernández
 453 et al., 2013], Diffusion Maps [Coifman et al., 2005], and Markov State Models (MSMs) [Prinz et al.,
 454 2011, Bowman et al., 2014, Mardt et al., 2018], which discretize conformational space into metastable
 455 states and estimate transition probabilities. These approaches unify dimensionality reduction and
 456 kinetics estimation under a variational principle.

457 **Modeling Molecular Dynamics** More recently, coarse-grained and full-atom generative models
 458 have sought to reconstruct trajectories and sample new transitions [Arts et al., 2023, Charron et al.,
 459 2025, Kohler et al., 2023, Majewski et al., 2023, Lu et al., 2025, Raja et al., 2025]. Methods such as
 460 score-based modeling [Daigavane et al., Tan et al., 2025], energy-based modeling [Lu et al., 2025,
 461 Lewis et al., 2025b], and flow-based generative dynamics [Jing et al., 2024, Kohler et al., 2023,
 462 Rehman et al., 2025] attempt to bypass explicit force fields by directly learning mappings between
 463 metastable ensembles.

464 **Schrödinger Bridge over MSM** In discrete time, classical Schrödinger Bridges (SBs) on Markov
 465 chains [Beghi, 2002, Pavon et al., 2010, Pavon and Ticozzi, 2010] solve endpoint-constrained path-
 466 space maximum-entropy problems by a multiplicative Doob h -transform of a prior kernel, with
 467 potentials given by space-time harmonic functions and uniqueness via the Beurling-Jamison theorem.
 468 While this theory provides constructive formulas for tilting Markov kernels analytically, **ScooBDoob**
 469 learns these tiltings directly from molecular dynamics trajectories. The student kernel \mathbf{P}_θ acts as a
 470 parametric Doob h -transform, constrained by reversibility and conditioned on metastable endpoints.

471 Whereas SBs enforce exact marginals and admit closed-form harmonic potentials, **ScooBDoob**
 472 enforces macrostate marginals and learns an approximate bridge distribution, extending the maximum
 473 entropy principle into a data-driven regime. Thus, given an MSM prior \prod and endpoint marginals
 474 (μ_0, μ_N) , with μ_N concentrated on a target macrostate, ScooBDoob seeks a Markov bridge kernel
 475 \mathbf{P}_θ that approximates the SB minimizer $\mathbb{P}^{\text{SB}} = \min_{\mathbb{P}} \{\text{KL}(\mathbb{P} \parallel \mathbb{Q}) : \mathbb{P}_0 = \mu_0, \mathbb{P}_N = \mu_N\}$ by training
 476 \mathbf{P}_θ to match the Doob-tilted optimum through MSM consistent losses.

477 **Learning Schrödinger Bridges** Schrödinger bridge methods have also been used outside molecular
 478 dynamics to construct samplers or generative models in continuous time. Bernton et al. [2019]
 479 approximates iterative proportional fitting in continuous state spaces to reduce variance in Annealed
 480 Importance Sampling and Sequential Monte Carlo. With others [De Bortoli et al., 2021, Liu et al.,
 481 2023] connect bridge dynamics with score-based generative modeling and Kim et al. [2024] extend
 482 the scope into graph transformation. While these methods focus on sampling from static or structured
 483 distributions via continuous or discrete diffusions, our approach differs in that we operate on finite-
 484 state MSMs and learn bridge kernels directly from MD trajectories to generate endpoint-conditioned
 485 paths between metastable states.

486 B Extended Theoretical Background

487 Here, we describe preliminaries and additional details on the theory of Schrödinger bridge matching
 488 with Doob's h -Transform and optimization on the Stiefel manifold.

489 B.1 Learning Discrete Schrödinger Bridges

490 **Schrödinger Bridge Problem** The Schrödinger Bridge (SB) problem aims to find the *optimal*
 491 probability path measure \mathbb{P} from samples of an initial distribution $\mathbf{x}_0 \sim \mu_0$ to samples from a final
 492 distribution $\mathbf{x}_N \sim \mu_N$. The optimal solution is defined as the path measure \mathbb{P}^{SB} with marginals μ_0
 493 and μ_N that minimizes the KL-divergence to a reference path measure \mathbb{Q}

$$\mathbb{P}^{\text{SB}} = \min_{\mathbb{P}} \{\text{KL}(\mathbb{P} \parallel \mathbb{Q}) : \mathbb{P}_0 = \mu_0, \mathbb{P}_N = \mu_N\} \quad (19)$$

494 where \mathbb{Q} can be defined as standard Brownian motion in continuous state spaces and a Dirichlet
 495 process in discrete state spaces. Note that $\mathbb{P}^{\text{SB}} \neq \mathbb{Q}$ as \mathbb{P} , since it must satisfy the boundary constraints
 496 $\mathbb{P} = \mu_0$ and $\mathbb{P}_T = \mu_T$.

497 **Continuous-Time Markov Chains** In discrete state spaces $\mathcal{X} = \{1, \dots, m\}$, time-varying stochastic
 498 process $(\mathbf{X}_t)_{t \in [0, T]}$ over the time horizon $[0, T]$ is considered a **continuous-time Markov chain**
 499 (**CTMC**) if it can be characterized by a transition rate matrix or *generator* $\mathbf{Q}_t \in \mathbb{R}^{\mathcal{X} \times \mathcal{X}}$ defined as

$$\mathbf{Q}_t(x, y) = \lim_{\Delta t \rightarrow 0} \frac{1}{\Delta t} [\mathbb{P}(\mathbf{X}_{t+\Delta t} = y | \mathbf{X}_t = x) - \mathbf{1}_{x=y}] \quad (20)$$

500 where $\mathbb{P}(\mathbf{X}_{t+\Delta t} = y | \mathbf{X}_t = x)$ is the probability of making a discrete "jump" from state x at time t
 501 to state y at time $t + \Delta t$ and $\mathbf{1}_{x=y}$ is an indicator function that equals 1 if $x = y$. By taking the limit
 502 as Δt , the generator defines the *instantaneous* jump probability at time t . By definition, all entries of
 503 the generator are non-negative for $x \neq y$ (i.e., $\mathbf{Q}_t(x, y) \geq 0$) and the diagonal entries are defined as
 504 $\mathbf{Q}_t(x, x) = - \sum_{y \neq x} \mathbf{Q}_t(x, y)$.

505 **Doob's h -Transform** The Doob's h -transform is a theoretically-grounded method to condition a
 506 transition rate matrix (or *generator*) $\mathbf{Q}_t(x, y) \in \mathbb{R}^{m \times m}$ of a CTMC $(\mathbf{X}_t)_{t \in [0, T]}$ to a target state z at

507 time T by *tilting* it via the conditional probability function $h_t(\mathbf{x})$.

$$\mathbf{Q}_t(x, y; z) = \mathbf{Q}_t(x, y) \frac{\mathbb{P}(\mathbf{X}_T = z | \mathbf{X}_t = y)}{\mathbb{P}(\mathbf{X}_T = z | \mathbf{X}_t = x)} - \delta_{xy} \sum_u \mathbf{Q}_t(x, u) \frac{\mathbb{P}(\mathbf{X}_T = z | \mathbf{X}_t = u)}{\mathbb{P}(\mathbf{X}_T = z | \mathbf{X}_t = x)} \quad (21)$$

508 where $\mathbb{P}(\mathbf{X}_T = z | \mathbf{X}_t = y)$ is the conditional probability of transitioning to a state z at time t given the current state $\mathbf{X}_t = x$ and δ_{xy} is the Dirac delta function that returns 1 when $x = y$ and 0 otherwise. Intuitively, this transform decreases the transition rate $x \rightarrow y$ if the probability of transitioning to z from state x is higher than from state y and increases the transition rate if the probability of transitioning to z from state y is higher than from state x .

513 B.2 Markov State Models

514 **Molecular Dynamics** A molecular dynamics (MD) simulation produces a time-ordered trajectory
 515 of molecular conformations, represented as Cartesian positions at discrete timesteps [Scherer et al.,
 516 2015]. For larger biomolecules, the dimensionality of the MD features grows prohibitively large,
 517 resulting in computational bottlenecks when simulating their trajectories. Coarse-graining techniques
 518 have aimed to lower the dimensionality of MD features by finding *collective variables* (CVs) that
 519 largely capture the degrees of freedom of a molecule's conformation over time [Ingólfsson et al.,
 520 2014, Joshi and Deshmukh, 2021].

521 **Time-lagged Independent Component Analysis (TICA)** Time-lagged independent component
 522 analysis (TICA; Pérez-Hernández et al. [2013]) is a method for reducing the high-dimensional feature
 523 space of molecular systems to a set of Collective Variables (CVs) that determine the primary degrees
 524 of freedom responsible for the slow transitions in MD simulations. Consider an MD snapshot of a
 525 d -dimensional molecular system at time t as $\mathbf{x}(t) \in \mathbb{R}^d$. Then, the time-lagged covariance matrices
 526 are defined as

$$\text{Cov}_{00} = \mathbb{E}[\mathbf{x}(t)\mathbf{x}(t)^\top], \quad \text{Cov}_{0\tau} = \mathbb{E}[\mathbf{x}(t)\mathbf{x}(t+\tau)^\top] \quad (22)$$

527 where the expectation is over the trajectory frames and τ is the chosen lag time. To determine the
 528 CVs, TICA solves the generalized eigenproblem

$$\text{Cov}_{0\tau} \mathbf{u}_i = \lambda_i \text{Cov}_{00} \mathbf{u}_i, \quad i \in \{1, \dots, d\} \quad (23)$$

529 where $\mathbf{u}_i \in \mathbb{R}^d$ are the eigenvectors and λ_i are the corresponding eigenvalues, and $t = -\tau / \ln \lambda_i$.
 530 With the top k eigenvalues sorted as $1 = |\lambda_1| \geq |\lambda_2| \geq \dots \geq |\lambda_d|$, we construct a projection matrix
 531 $\mathbf{U} \in \mathbb{R}^{n \times k}$ with columns being the corresponding eigenvectors, which projects $\mathbf{x}(t) \in \mathbb{R}^d$ to a
 532 k -dimensional feature vector $\mathbf{y}(t)$ as

$$\mathbf{y}(t) = \mathbf{U}^\top \mathbf{x}(t), \quad \mathbf{U} = [\mathbf{u}_1, \dots, \mathbf{u}_k] \quad (24)$$

533 **Constructing the Markov State Model** We can cluster the TICA-projected $\mathbf{y}(t)$ into m discrete
 534 microstates and represent state transitions over a lag time τ by a **Markov State Model (MSM)**.
 535 Formally, an MSM at lag time τ is defined as a stochastic matrix $\mathbf{P}(\tau) \in \mathbb{R}^{m \times m}$ matrix of transition
 536 probabilities:

$$\mathbf{P}(\tau) \in \mathbb{R}^{m \times m}, \quad \mathbf{P}_{ij}(\tau) = \mathbb{P}(\mathbf{X}_{t+\tau} = j | \mathbf{X}_t = i) = \frac{C(i, j; \tau)}{\sum_{j'} C(i, j'; \tau)}, \quad (25)$$

537 where $C(i, j; \tau)$ is the observed count of transitions from state i at time t to state j at time $t + \tau$. The
 538 construction of an MSM has a natural connection to CTMCs, where the transition probabilities define
 539 a stochastic trajectory between discrete micro-states, which motivates our work.

540 B.3 Stiefel Manifold Constraint

541 **Stiefel Manifold** The Stiefel manifold, denoted $\mathcal{S}_{n,k}$ is the set of $n \times k$ ($n \geq k$) orthonormal
 542 rectangular matrices defined as

$$\mathcal{S}_{n,k} = \{\mathbf{Q} \in \mathbb{R}^{n \times k} | \mathbf{Q}^\top \mathbf{Q} = \mathbf{I}_k\} \quad (26)$$

543 where $\mathbf{I}_k \in \mathbb{R}^{k \times k}$ is the $k \times k$ identity matrix.

544 **Eigendecomposition of MSM** Given the MSM transition matrix $\mathbf{P}(\tau)$ at lag time τ , there exists a
 545 *stationary distribution* $\boldsymbol{\pi} \in \mathbb{R}^m$ such that $\mathbf{P}(\tau)\boldsymbol{\pi} = \boldsymbol{\pi}$ [Beauchamp et al., 2011]. Symmetrize via:

$$\mathbf{M} = \mathbf{D}^{\frac{1}{2}} \mathbf{P}(\tau) \mathbf{D}^{-\frac{1}{2}}, \quad \mathbf{D} = \text{diag}(\boldsymbol{\pi}) \quad (27)$$

546 We then diagonalize

$$\mathbf{M} = \mathbf{Q}_{\text{MSM}} \boldsymbol{\Lambda}_{\text{MSM}} \mathbf{Q}_{\text{MSM}}^\top, \quad \mathbf{Q}_{\text{MSM}} \in \mathbb{R}^{m \times r}, \quad \boldsymbol{\Lambda}_{\text{MSM}} = \text{diag}(\lambda_1, \dots, \lambda_m), \quad (28)$$

547 so that

$$\mathbf{P}(\tau) = \mathbf{D}^{-\frac{1}{2}} \mathbf{Q}_{\text{MSM}} \boldsymbol{\Lambda}_{\text{MSM}} \mathbf{Q}_{\text{MSM}}^\top \mathbf{D}^{\frac{1}{2}} = \sum_{i=1}^m \lambda_i \mathbf{r}_i \mathbf{\ell}_i^\top, \quad (29)$$

548 where λ_i are the eigenvalues of $\mathbf{P}(\tau)$, and \mathbf{r}_i and $\mathbf{\ell}_i$ are the corresponding right and left eigenvectors,
 549 respectively. $\mathbf{r}_i = \mathbf{D}^{-\frac{1}{2}} \mathbf{q}_i$, $\mathbf{\ell}_i = \mathbf{D}^{\frac{1}{2}} \mathbf{q}_i$, and bi-orthogonality $\mathbf{\ell}_i^\top \mathbf{D} \mathbf{r}_j = \delta_{ij}$ maintains.

550 B.4 Chapman-Kolmogorov Consistency

551 For a Markov chain modeling of dynamics at lag time τ , one step of length $k\tau$ should look the same
 552 as k consecutive steps of length τ .

$$\mathbf{P}(k\tau) = \mathbf{P}(\tau)^k, \quad k = 2, 3, \dots \quad (30)$$

553 If such CK consistency fails, the assumption that the dynamics are approximately Markovian at lag τ
 554 does not hold.

555 From the MD trajectory, count matrix C_{ij} can be built to represent jump from state i to state j after
 556 lag τ . Assume that at lag $k\tau$ there exists $C_{k\tau}$, counts can be turned into probability:

$$\hat{\mathbf{P}}_{\text{ref}}(\tau)[i, j] = \frac{C_\tau[i, j]}{\sum_{j'} (C_\tau[i, j'])} \quad (31)$$

557 where $j = k$ depend on the metrics asked. ScoobDoob parameterizes the one-step kernel P_θ , and the
 558 CK consistency is used to measure whether

$$\mathbf{P}_\theta^k \approx \hat{\mathbf{P}}_{\text{ref}}(k\tau). \quad (32)$$

559 Low CK error indicates that the learned one-step dynamics compose correctly over longer lags, a
 560 prerequisite for stable implied timescales and reliable kinetic predictions [Prinz et al., 2011, Bowman
 561 et al., 2014, Noé and Clementi, 2017].

562 C Theoretical Proofs

563 **Lemma 1** (Row-stochasticity and telescoping identity). *Let $\mathbf{P}(\tau) \in \mathbb{R}^{m \times m}$ be a row-stochastic
 564 MSM transition matrix and let $(\mathbf{h}_n)_{n=0}^N$ be the backward sequence defined by*

$$\mathbf{h}_N = \nu, \quad \mathbf{h}_n = \mathbf{P}(\tau) \mathbf{h}_{n+1}, \quad n = N-1, \dots, 0,$$

565 *or, in the density-aware case, by*

$$\mathbf{h}_N^V = \nu, \quad \mathbf{h}_n^V = \mathbf{P}(\tau) \text{diag}(\mathbf{w}) \mathbf{h}_{n+1}^V, \quad n = N-1, \dots, 0,$$

566 *with $w_j = \exp(-\tau V(j))$ as in Section 2.2. Define the time-inhomogeneous Doob kernels*

$$\mathbf{P}_n^h(i, j) = \frac{\mathbf{P}_{ij}(\tau) \mathbf{h}_{n+1}(j)}{\mathbf{h}_n(i)}, \quad \text{or} \quad \mathbf{P}_n^h(i, j) = \frac{\mathbf{P}_{ij}(\tau) w_j \mathbf{h}_{n+1}^V(j)}{(\mathbf{P}(\tau) \text{diag}(\mathbf{w}) \mathbf{h}_{n+1}^V)(i)}.$$

567 *Then for every n and i , $\sum_j \mathbf{P}_n^h(i, j) = 1$ (row-stochasticity). Moreover, for any path (i_0, \dots, i_N)
 568 the path probability under the Doob chain satisfies the telescoping identity*

$$\mu_0(i_0) \prod_{n=0}^{N-1} \mathbf{P}_n^h(i_n, i_{n+1}) = \mu_0(i_0) \left(\prod_{n=0}^{N-1} \mathbf{P}_{i_n i_{n+1}}(\tau) \right) \cdot \frac{\mathbf{h}_N(i_N)}{\mathbf{h}_0(i_0)},$$

569 *with \mathbf{h}_n replaced by \mathbf{h}_n^V in the density-aware case. Row-stochasticity is immediate from the weighted
 570 space-time harmonic relation $\mathbf{h}_n = \mathbf{P}(\tau) \text{diag}(\mathbf{w}) \mathbf{h}_{n+1}$ (cf. Pavon-Ticozzi, Eq 25) [Pavon and Ticozzi,
 571 2010], exactly as in their Eq. 27, where $\sum_j \hat{p}_{ij} = 1$ follows by dividing $\sum_j \pi_{ij} \varphi(t+1, j)$ by $\varphi(t, i)$.*

572 *Proof.* Row-stochasticity follows from the backward recursion, where we sum over columns j :

$$\sum_j^m \mathbf{P}_n^h(i, j) = \frac{1}{\mathbf{h}_n(i)} \sum_j^m \mathbf{P}_{ij}(\tau) \mathbf{h}_{n+1}(j) = \frac{(\mathbf{P}(\tau) \mathbf{h}_{n+1})(i)}{\mathbf{h}_n(i)} = \frac{\mathbf{h}_n(i)}{\mathbf{h}_n(i)} = 1,$$

573 and similarly in the density-aware case with $\text{diag}(\mathbf{w}) \mathbf{h}_{n+1}^V$. For the telescoping identity, expand the
574 product of Doob factors and note that the ratios $\mathbf{h}_{n+1}(i_{n+1})/\mathbf{h}_n(i_n)$ cancel along the path, leaving
575 only $\mathbf{h}_N(i_N)/\mathbf{h}_0(i_0)$. The argument is identical with \mathbf{h}^V . \square

Proposition 2.1 (ScooBDoob yields the target end state for one-hot ν). *Assume the terminal distribution is the one-hot vector $\nu = \mathbf{e}_z$ concentrating all mass on a fixed target microstate z . Let \mathbf{h}_n (or \mathbf{h}_n^V) be defined by the backward recursions above and let \mathbf{P}_n^h be the corresponding Doob kernels. For any initial distribution μ_0 supported on $\{i : \mathbf{h}_0(i) > 0\}$, the forward evolution*

$$\mu_{n+1} = \mu_n \mathbf{P}_n^h, \quad n = 0, 1, \dots, N-1$$

576 *at terminal time satisfies $\mu_N = \nu$.*

577 *Proof.* We prove the density-aware case (the unweighted case is identical with $w_j \equiv 1$). Since
578 $\nu = \mathbf{e}_z$, we have

$$\mathbf{h}_N^V = \nu = \mathbf{e}_z, \quad \mathbf{h}_{N-1}^V = \mathbf{P}(\tau) \text{diag}(\mathbf{w}) \mathbf{e}_z = w_z \mathbf{P}(\tau) \mathbf{e}_z,$$

579 so that $\mathbf{h}_{N-1}^V(i) = w_z \mathbf{P}_{iz}(\tau)$ for every i . By Eq. (5), for the final step $n = N-1$ and any i, j ,

$$\mathbf{P}_{N-1}^h(i, j) = \frac{\mathbf{P}_{ij}(\tau) w_j \nu(j)}{w_z \mathbf{P}_{iz}(\tau)} = \delta_{jz} = \begin{cases} 1, & j = z, \\ 0, & j \neq z. \end{cases}$$

580 Thus the last-step kernel \mathbf{P}_{N-1}^h deterministically sends all mass into z , so regardless of μ_{N-1} ,

$$\mu_N(j) = \sum_i^m \mu_{N-1}(i) \mathbf{P}_{N-1}^h(i, j) = \sum_i^m \mu_{N-1}(i) \delta_{jz} = \delta_{jz} = \mathbf{e}_z = \nu(j).$$

581 where δ is the Kronecker delta. Because each \mathbf{P}_n^h is row-stochastic (Lemma 1), normalization and
582 positivity are preserved throughout, and the recursion is well defined for all n . Hence $\mu_N = \nu$. \square

583 **Remark 1** (General terminal distributions). *For a general terminal law $\nu \in \Delta^{m-1}$ (not necessarily
584 one-hot), the Doob kernels (Eqs. (2) or (5)) still define a valid inhomogeneous Markov chain. Writing
585 $\alpha_n(i) := \mu_n(i)/\mathbf{h}_n(i)$ (or $\alpha_n(i) := \mu_n(i)/\mathbf{h}_n^V(i)$ in the density-aware case). Then one verifies that
586 $\alpha_{n+1}^\top = \alpha_n^\top \mathbf{P}(\tau)$ (unweighted), $\alpha_{n+1}^\top = \alpha_n^\top \mathbf{P}(\tau) \text{diag}(\mathbf{w})$ (density-aware). Hence*

$$\mu_N(j) = \nu(j) [\alpha_0^\top \mathbf{P}(\tau)^N]_j \quad \text{or} \quad \mu_N(j) = \nu(j) [\alpha_0^\top (\mathbf{P}(\tau) \text{diag}(\mathbf{w}))^N]_j$$

587 To enforce $\mu_N = \nu$ componentwise for arbitrary μ_0 , one requires the full Schrödinger system
588 (maximum-entropy) compatibility between the boundary marginals, equivalently choosing the forward
589 potential so that the terminal factor equals 1; see Appendix A.3 and Eq. (24). In our experiments we
590 restrict to the one-hot terminal law (Appendix D.1), for which Proposition 2.1 applies directly.

591 D Additional Results and Discussion

592 D.1 Evaluating Spectral Stability During Training

593 **Spectral gap** Denote the symmetrized operator by $\mathbf{M} \in \mathbb{R}^{m \times m}$ with eigenvalues $1 = \lambda_1 \geq \lambda_2 \geq \dots \lambda_m$. The spectral gap is the difference between $\lambda_1 - \lambda_2$, which quantifies separation between
594 the stationary mode and the slowest dynamic process [Prinz et al., 2011]. A larger gap is a clearer
595 metastable separation.

Table A1: **Zero-shot evaluation across temperatures.** Metrics computed at replicas 412 K and 503 K using models trained at 400 K. Lower is better. Multi- N maintains CK consistency with only a modest increase in KL.

Model	412 K			503 K		
	Row-KL	CK	\mathcal{W}_2	Row-KL	CK	\mathcal{W}_2
Fixed- N	1.462	0.925	0.016	1.047	0.869	0.041
Multi- N	1.520	0.927	0.020	1.124	0.877	0.023



Figure A1: **Spectral stability metrics over training steps.**

Table A2: Spectral stability diagnostics of the learned MSM during training. All metrics indicate stable eigenvalues and eigenvectors across training, attributed to the Stiefel constraints.

Metric	Value (mean \pm std)
Spectral gap (gap_1)	0.091 ± 0.014
Perron eigenvalue (λ_1)	1.000028 ± 0.000001
Overlap diag. mean (\uparrow)	0.951 ± 0.084
Overlap diag. min (\uparrow)	0.829 ± 0.340
Residual (first eigenpair) (\downarrow)	$(1.9 \pm 0.3) \times 10^{-5}$
Residual (mean top- r) (\downarrow)	$(2.3 \pm 0.1) \times 10^{-5}$
Subspace distance (SubF) (\downarrow)	0.341 ± 0.494

597 **Perron eigenvalue** For any row-stochastic transition matrix, the Perron-Frobenius theorem guarantees a leading eigenvalue $\lambda_1 = 1$. Deviations indicate difficulty in normalization and reversibility of
598 $P_\theta(\tau)$ [Smyth, 2002].

600 **Overlap diag.** Let $\mathbf{Q}_{\text{MSM}}^{(t)}$ and $\mathbf{Q}_{\text{MSM}}^{(t-1)}$ denote the top r eigenvectors of M at successive training
601 steps. The overlap matrix $\mathbf{O} = (\mathbf{Q}_{\text{MSM}}^{(t-1)})^\top \mathbf{Q}_{\text{MSM}}^{(t)}$ measures alignment [Husic and Pande, 2018]. The
602 mean and minimum of the diagonal entries of $|\mathbf{O}|$ indicates how stable each eigenvector is across
603 epochs.

604 **Residual** For each eigenpair $(\lambda_i, \mathbf{q}_i)$ with \mathbf{q}_i a column of \mathbf{Q}_{MSM} , the residual is defined follows
605 Simoncini [2005] as

$$\|\mathbf{M}\mathbf{q}_i - \lambda_i \mathbf{q}_i\|_2. \quad (33)$$

606 Small numbers confirms that the computed eigenpairs solve the eigenvalue problem accurately.

607 **Subspace distance** The subspace spanned between epochs by the top r eigenvectors is represented
608 by the projection matrix $\mathbf{Q}_{\text{MSM}} \mathbf{Q}_{\text{MSM}}^\top$. Subspace distance between two consecutive steps is measured
609 as the Frobenius norm

$$\left\| \mathbf{Q}_{\text{MSM}}^{(t)} (\mathbf{Q}_{\text{MSM}}^{(t)})^\top - \mathbf{Q}_{\text{MSM}}^{(t-1)} (\mathbf{Q}_{\text{MSM}}^{(t-1)})^\top \right\|_F, \quad (34)$$

610 which is invariant to rotations and sign flips. Smaller values indicate that the slow kinetic subspace is
611 stable across training iterations.

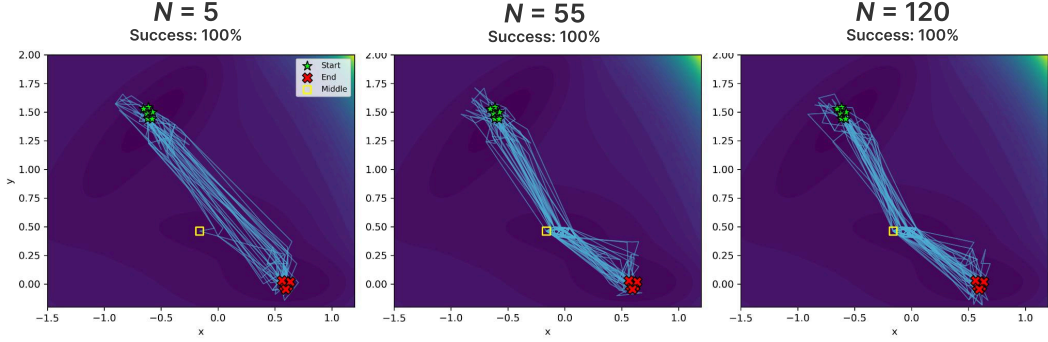


Figure A2: **Transition Paths Predicted by ScooBDoob on Müller-Brown Potential.** Tested path generation on unseen number of steps N . Green stars indicate starting states and red Xs indicate target end state. Intermediate transition states are marked with the yellow square.

612 E Experimental Details

613 E.1 Automatic τ Sweeping and Endpoint Determination

614 For systems like AIB9 where inputs are torsion features without clear labels for start and end
 615 microstates, we avoid manual choices and infer 1) a suitable lag time τ and 2) representative start/end
 616 state sets directly from kinetics estimated on the data.

617 Based on our previous discussion on MSMs, the pair (λ_2, q_2) encodes the slowest nontrivial relaxation.
 618 We use the sign of the second eigenvector q_2 to produce a coarse two-well split [Röblitz and Weber,
 619 2013]:

$$\mathcal{A} = \{i : (q_2)_i \leq 0\}, \quad \mathcal{B} = \{i : (q_2)_i > 0\}. \quad (35)$$

620 To get confident endpoints for conditioning, we then pick the k most negative entries of q_2 as the
 621 start set S_{start} and the k most positive as the end set S_{end} . In the current experiment, k is set to 6.

622 For a chosen lag τ , the implied timescale of the slowest process is

$$t_2(\tau) = \frac{-\tau}{\ln |\lambda_2|}, \quad \text{spectral_gap} = 1 - |\lambda_2|. \quad (36)$$

623 A larger gap implied clearer separation between the stationary mode and the slowest transition, which
 624 tends to stabilize metastable assignments.

625 A grid of lag steps τ_{multiple} range from 40 to 200 was tested. The final τ will be picked by maximizing
 626 the score below that favors both kinetic separation and a split with balanced start and end states:

$$\text{score}(\tau) = \text{spectral_gap}(\tau)(0.5 + 0.5 \cdot \frac{\min(|\mathcal{A}|, |\mathcal{B}|)}{\max(1, \max(|\mathcal{A}|, |\mathcal{B}|))}) \quad (37)$$

627 Then during training, at τ^* we set $S_{\text{start}}/S_{\text{end}}$ to the k most negative/positive entries of q_2 .

628 E.2 Constructing the Teacher Transition Matrix

629 The teacher transition matrix $\mathbf{P}_{\text{ref}}(\tau)$ is used to define the matching objective of the parameterized
 630 student model $\mathbf{P}_{\theta}(\tau)$. We fix a time horizon $T = N\tau$ and a terminal distribution $\nu \in \Delta^{m-1}$, where
 631 N is the number of lag steps. For a target state z , we set the terminal distribution to the one-hot
 632 vector. We define the conditional distributions at each time step $\mathbf{h}_n^V \in \Delta^{m-1}$ as

$$\mathbf{h}_N = \nu, \quad \mathbf{h}_n = \mathbf{P}_{\text{ref}}(\tau) \text{diag}(\mathbf{w}) \mathbf{h}_{n+1}, \quad n \in \{N-1, \dots, 0\}. \quad (38)$$

633 The Doob h -transformed teacher transition matrices at each time step are then defined as

$$\mathbf{P}_{\text{ref},n}^h(i, j) = \frac{\mathbf{P}_{\text{ref}}(i, j; \tau) \mathbf{w}(j) \mathbf{h}_{\theta, n+1}(j)}{(\mathbf{P}_{\text{ref}}(\tau) \text{diag}(\mathbf{w}) \mathbf{h}_{\theta, n+1})(i)} \quad (39)$$

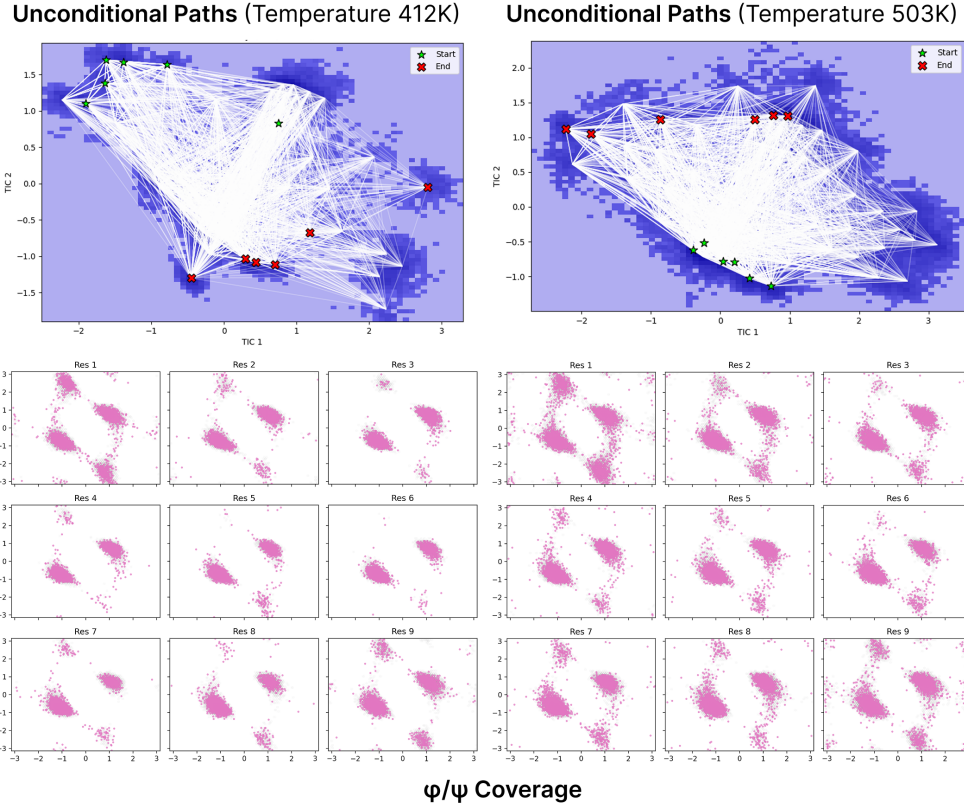


Figure A3: **Unconditional transition paths of Aib9 peptide at temperatures of 412K and 503K.** Simulations were performed with trained models under the identical conditions of $K = 40$ and $N = 60$. **Above:** Darker color indicates lower-energy states, with white lines showing sampled transition paths. Start and End states were determined following Appendix E. **Below:** Color highlights the states visited by the model. The grey background indicates ground-truth coverage.

634 E.3 Data Curation

635 **Synthetic Müller-Brown Potential** Following [Müller and Brown, 1979], we build up the testing
 636 system for a 2D and 3D Müller-Brown potential with a potential energy landscape $U(\mathbf{x})$ with three
 637 local minima states.

$$U(\mathbf{x}) = \sum_{j=1}^4 A_j \cdot \exp[a_j(x_1 - X_j)^2 + b_j(x_1 - Y_j)(x_2 - X_j) + c_j(x_2 - Y_j)^2] \quad (40)$$

638 where $a = (-1, -1, -6.5, -0.7)$, $b = (0, 0, 11, 0.6)$, $c = (-10, -10, -6.5, 0.7)$, $A =$
 639 $(-200, -100, -170, 15)$, $X = (1, 0, -0.5, -1)$, $Y = (0, 0.5, 1.5, 1)$, as formulated in [Müller
 640 and Brown, 1979, Hernández et al., 2018]. The dynamics are governed by

$$\dot{\mathbf{x}}(t) = -\beta \nabla U(\mathbf{x}) + \sqrt{2D} \eta(t) \quad (41)$$

641 where $\beta = 1$, $\eta(t)$ is Gaussian noise with zero mean, time step $\Delta t = 10^{-3}$, and reflecting bounds
 642 $(-1.5, 1.2) \times (-0.2, 2.0)$.

643 E.4 Loss Construction

644 We used a complex loss system to maintain the Markov State Model properties. Additional constraints
 645 like the Chapman-Kolmogorov loss ensure the conservation of the stationary distribution at the second-
 646 highest eigenvalue. Reversibility loss ensures that the detailed balance is held in the MSM system,
 647 and the Stiefel constraint ensures that the eigenvectors remain orthogonal.

648 For protein systems, the K can be large with thousands of states, so we approximate the \mathbf{P}_θ by only
 649 predicting the transition probabilities for the $k = 48$ nearest neighbors:

$$\forall j \in \mathcal{N}(i), \quad \mathbf{P}_\theta(i, j) = \text{softmax}(p_\theta(\mathbf{z}_i, \mathbf{z}_j; n)) \quad (42)$$

650 where $\mathcal{N}(i)$ are the k nearest neighbors of state i .

651 E.5 Training Details

652 For MB potential training, a two-layer MLP with a hidden dimension of 128 and a dropout rate of
 653 0.1 was used to map the features to a scalar score. We trained the model for 200 epochs with early
 654 stopping. The learning rate was set to $3e^{-3}$ using the Adam optimizer. All default hyperparameters
 655 are given in Table A3.

656 For Aib9 peptide experiments, we concatenated all angle features into a $36D$ -shaped input for the
 657 model, and applied a 2-layer MLP encoder that takes paired interaction features as input. The learning
 658 rate was set to $1e^{-3}$ using the Adam optimizer. Training occurred for 200 epochs with early stopping.
 659 All default hyperparameters are given in Table A3.

Table A3: Default hyperparameters for MB and Aib9 peptide experiments.

Experiment	Δt	Temp (K)	LR	Epochs	λ_{CK}	λ_{rev}	λ_{stf}	λ_{br}	Paths (unc/cond)
MB Potential	1.0×10^{-3}	–	1×10^{-3}	200	1.0	1.0	1.0	1.0	200 / 200
Aib9 Peptide	2.0 ps	400	1×10^{-3}	200	1.0	2.0	2.0	1.0	100 / 100

660 E.6 Evaluation Metrics

661 **Row-KL Divergence** We evaluate the KL-divergence of the predicted transition probabilities from
 662 each micro-state $i \in \{1, \dots, m\}$ defined as a row of the parameterized transition matrix $\mathbf{P}_\theta(\tau)$
 663 compared to the teacher transition matrix $\mathbf{P}_{\text{ref}}(\tau)$.

$$D_{\text{KL}}(\mathbf{P}_\theta(i, \cdot) \parallel \mathbf{P}_{\text{ref}}(i, \cdot)) = \sum_{j=1}^m \mathbf{P}_\theta(i, j) \log \frac{\mathbf{P}_\theta(i, j)}{\mathbf{P}_{\text{ref}}(i, j)} \quad (43)$$

664 **Wasserstein-2 Distance (\mathcal{W}_2)** We compute the \mathcal{W}_2 distance of the predicted terminal state

$$\mathcal{W}_2 = \left(\min_{\pi \in \Pi(p, q)} \int \|\mathbf{x} - \mathbf{y}\|_2^2 d\pi(\mathbf{x}, \mathbf{y}) \right)^{1/2} \quad (44)$$

665 **Chapman-Kolmogorov Error** We are comparing the student kernel \mathbf{P}_θ at lag τ against empirical
 666 2-lag kernel from counts to satisfy:

$$\mathbf{P}(2\tau) = \mathbf{P}(\tau)^2 \quad (45)$$

667 The error is reported to be:

$$\frac{\|\mathbf{P}_\theta^2 - \mathbf{P}_{\text{ref}}(2\tau)\|_F}{\max(10^{-16}, \|\mathbf{P}_{\text{ref}}(2\tau)\|_F)} \quad (46)$$

668 If the error is small, the model composes correctly and respect Markovianity, otherwise the model is
 669 not consistent across time lags.

670 **F Algorithms**

671 Here, we provide the pseudocode for the construction of the teacher transition matrices and training
 672 the parameterized time-dependent generators in Algorithm 2 and the procedure for simulating the
 unconditional and target-conditioned dynamics with ScooBDoob in Algorithm 3.

Algorithm 2 Training ScooBDoob

```

1: Input: Observed count of transitions between states  $i \rightarrow j$  at  $\tau$  lag  $C(i, j; \tau)$  for all  $i, j \in \{1, \dots, m\}$ 
2: while Training do
3:    $\mathbf{P}_{ij}(\tau) \leftarrow \frac{C(i, j; \tau)}{\sum_{j'} C(i, j'; \tau)}$   $\triangleright$  compute transition probabilities from each microstate
4:    $\mathbf{P}(\tau) \leftarrow [\mathbf{P}_{ij}(\tau)]$   $\triangleright$  construct unconditional transition matrix
5:    $\mathbf{V}(i) \leftarrow \alpha/(C_i + 1)$ ,  $\mathbf{w}(i) \leftarrow \exp(-\tau \mathbf{V}(i))$   $\triangleright$  density-aware weights
6:    $\mathbf{h}_N^V \leftarrow \nu$   $\triangleright$  initialize terminal condition
7:   for  $n$  in  $N - 1, \dots, 0$  do
8:      $\mathbf{h}_n^V \leftarrow \mathbf{P}(\tau)(\text{diag}(\mathbf{w})\mathbf{h}_{n+1}^V)$   $\triangleright$  compute tilted distributions
9:      $\mathbf{P}_n^V(i, j) \leftarrow \frac{\mathbf{P}_{ij}(\tau)\mathbf{w}(j)\mathbf{h}_{n+1}^V(j)}{(\mathbf{P}(\tau)\text{diag}(\mathbf{w})\mathbf{h}_{n+1}^V(i))}$   $\triangleright$  compute doob-tilted probabilities
10:     $\mathbf{P}_n^V \leftarrow [\mathbf{P}_n^V(i, j)]$   $\triangleright$  construct matrix
11:   end for
12:   for micro-state  $i$  in  $1, \dots, m$  do  $\triangleright$  train generator for each state  $i$ 
13:      $\mathbf{P}_{n,\theta}^h(i, \cdot) \leftarrow \text{NN}(\theta)$ 
14:     Compute loss  $\mathcal{L}_{\text{total}}(\theta) = \mathcal{L}_{\text{MSM}}(\theta) + \gamma_{\text{bridge}}\mathcal{L}_{\text{bridge}}(\theta) + \gamma_{\text{stief}}\mathcal{L}_{\text{stief}}(\theta)$ 
15:     Optimize  $\theta$  with  $\nabla_{\theta}\mathcal{L}_{\text{total}}$ 
16:   end for
17: end while
20: return parameterized transition predictor  $\mathbf{P}_{\theta}(\tau) : [0, 1] \rightarrow \mathbb{R}^{m \times m}$ 

```

673

Algorithm 3 Inference with ScooBDoob

```

1: Input: parameterized model  $\mathbf{P}_{\theta}(\tau) : [0, 1] \rightarrow \mathbb{R}^{m \times m}$ , initial distribution  $\mu_0$ , number of steps  $N$ 
2:  $\mathcal{P} \leftarrow \{\}$   $\triangleright$  initialize path
3: for step  $n$  in  $1, \dots, N - 1$  do
4:    $\mu_n \leftarrow \mu_{n-1}\mathbf{P}_{\theta}(\tau)$   $\triangleright$  predict distribution over microstates
5:    $z_n \sim \mu_n$   $\triangleright$  sample discrete state from distribution
6:    $\mathcal{P} \leftarrow \mathcal{P} \cup \{\mu_n, z_n\}$   $\triangleright$  append to path
7: end for
8: return  $\mathcal{P}, \mu_N, z_n$ 

```
